
USING ECHO STATE NETWORKS TO INFORM PHYSICAL MODELS FOR FIRE FRONT PROPAGATION

Myungsoo Yoo*

University of Missouri
mym4v@mail.missouri.edu

Christopher K. Wikle

University of Missouri
wiklec@missouri.edu

ABSTRACT

Wildfires can be devastating, causing significant damage to property, ecosystem disruption, and loss of life. Forecasting the evolution of wildfire boundaries is essential to real-time wildfire management. To this end, substantial attention in the wildfire literature has focused on the level set method, which effectively represents complicated boundaries and their change over time. Nevertheless, most of these approaches rely on a heavily-parameterized formulas for spread and fail to account for the uncertainty in the forecast. The rapid evolution of large wildfires and inhomogeneous environmental conditions across the domain of interest (e.g., varying land cover, fire-induced winds) give rise to a need for a model that enables efficient data-driven learning of fire spread and allows uncertainty quantification. Here, we present a novel hybrid model that nests an echo state network to learn nonlinear spatio-temporal evolving velocities (speed in the normal direction) within a physically-based level set model framework. This model is computationally efficient and includes calibrated uncertainty quantification. We show the forecasting performance of our model with simulations and two real data sets - the Haybress and Thomas megafires that started in California (USA) in 2017.

Keywords wildfire · signed distance function · boundary · level set method · echo state network · spatio-temporal

1 Introduction

Wildfires can negatively affect natural and human ecosystems through loss of life, property damage, emission of air pollutants and impacts on water quality, among others (e.g., [Brotons et al., 2013](#); [Hohner et al., 2019](#)). Indeed, wildfires can continue to pose a risk even after they are extinguished. For instance, [Cannon and DeGraff \(2009\)](#) raised public awareness of the impact of the post-fire debris flow. As stake holders consider tradeoffs between managing

*Author of correspondence

ecosystems and preventing loss of life and property, having as much information to plan wildfire suppression tactics as early as possible is important. This requires an efficient and reliable forecasting model for the evolution of wildfires.

The level set method proposed by [Osher and Sethian \(1988\)](#) has become one of the most useful approaches for modeling the evolution of wildfire fronts in operational fire models (e.g., [Miller et al., 2015](#)). [Osher and Fedkiw \(2002\)](#) summarized various implementations of the level set method, and [Gibou et al. \(2018\)](#) provided a recent review. In the application to wildfire, the level set method frequently relies on heavily-parameterized quasi-empirical formulations of the wildfire front velocity, such as the Rothermel model ([Rothermel, 1972](#)). Such models can be suitable and perform well under homogeneous environmental and atmospheric conditions. For example, [Dabrowski et al. \(2022a\)](#) used the Rothermel model with an unknown parameter to inform velocity in the level set method by using an ensemble Kalman filter (EnKF). Similarly, [Mallet et al. \(2009\)](#) and [Alessandri et al. \(2021\)](#) simplified the velocity through formulas proposed by [Fendell and Wolff \(2001\)](#) and [Lo \(2012\)](#), respectively. None of these approaches utilizes a data-driven approach to learn the spatially and temporally varying front velocity over the entire domain, which is required for realistic front propagation in complex environments, especially where large fires create their own “weather”.

As discussed below, the implicit function used in the level set method to represent the fire boundary is a time-varying signed distance function that is referenced in space and time. Spatio-temporal data are ubiquitous in the environmental sciences and multi-level hierarchical representations have long been used to model such complex processes (e.g., see [Cressie and Wikle, 2011](#); [Banerjee et al., 2015](#), for general discussion). Likewise, the dependency observed in space or time has triggered intellectual curiosity in the deep learning community. [Wikle and Zammit-Mangion \(2022\)](#) provide a recent overview of statistical and AI approaches for deep learning spatial and spatio-temporal data. Convolutional neural networks (CNNs), recurrent neural networks (RNNs), and their variants are the primary approaches in the deep learning literature for such data. In particular, hybrid convolutional recurrent networks (e.g., [Zuo et al., 2015](#)) have worked well for spatio-temporal data. For example, in the context of wildfire, [Burge et al. \(2022\)](#) proposed the EPD-convLSTM model, which accounts for spatial and temporal dependency by combining a convolutional long short-term memory (LSTM) RNN and an Encoder-Processor-Decoder (EPD). However, these methods do not provide a mechanism for uncertainty quantification, do not directly incorporate physical relationships (such as implied by the level set method), and require a large amount of training data.

An enhancement to traditional deep learning neural network approaches is to use so-called “physics-informed neural networks” that seek to encode physical relationships into the deep neural architecture (e.g., [Raissi et al., 2019](#)). These methods have recently been considered for level-set fire front propagation in [Dabrowski et al. \(2022b\)](#). Their work is implemented in a Bayesian framework that allows for data assimilation and uncertainty quantification. However, this approach does not consider realistic data-driven spatial and temporally varying velocities or large-scale megafire spread, which is our interest here. Alternatively, [Yoo and Wikle \(2022\)](#) considered a hybrid physical/statistical level set model within a hierarchical Bayesian framework. Their approach included a latent vector autoregressive stochastic spatio-temporal process for velocity, and accommodates data assimilation and uncertainty quantification naturally in

the Bayesian inference paradigm. However, as with many spatio-temporal Bayesian models, this method is fairly computationally intensive and is somewhat limited in that the latent dynamical process is assumed to be linear.

We consider here an alternative approach for efficient physics-informed neural models that provides realistic data-driven estimates of fire front velocities as well as realistic uncertainty quantification. Specifically, we utilize a reservoir computing recurrent neural model known as an echo state network (ESN). Hybrid ESN/statistical approaches for spatio-temporal data were introduced into statistics by [McDermott and Wikle \(2017, 2019\)](#) and have subsequently been used in numerous applications (e.g., [Bonas and Castruccio, 2021](#); [Huang et al., 2021](#); [Barredo Arrieta et al., 2022](#)). Rather than estimate neural weight parameters, ESNs and other reservoir models draw weights randomly from a reservoir distribution, and only train the output layer parameters. This provides a distinct advantage over traditional neural models in that much less data is required to train ESNs, making them ideal for situations such as real-world fire spread where fire boundary data are only available sporadically (e.g., daily). As with most neural methods, two big challenges with ESNs relate to hyperparameter tuning (e.g., [Wu et al., 2018](#); [Probst et al., 2018](#)) and uncertainty quantification (e.g., [McDermott and Wikle, 2019](#)).

In this paper, we propose an ensemble ESN within the level set framework, which combines the mechanistically-motivated dynamic model (the level set method) with reservoir modeling (ESN) of velocities. There are several contributions of this work. Retaining the level set method as the physically-motivated dynamical core, our model enables a simple representation of any complicated boundary and its topological change through time. The ESN, nested within the level set method to learn propagation speeds, can improve forecasting performance by accommodating more complicated (i.e., nonlinear) dynamics that are present in many dynamic systems ([Chen and Billings, 1992](#)). Importantly, the low computational cost of ESNs makes our model suitable and attractive for practical use. In that regard, our method addresses the neural hyperparameter tuning issue efficiently by randomly sampling the hyperparameters from plausible distributions to construct forecast ensembles. Finally, our method can quantify the uncertainty in forecasting by using the ensembles with novel calibration. Compared to forecast intervals derived from the Bayesian approach of [Yoo and Wikle \(2022\)](#), our method provides less formal forecast intervals, but they are effective and much less computationally expensive. We demonstrate the forecasting performance of the model on two simulated datasets generated from actual wind fields and two wildfires in California – the Thomas and Haypress megafires.

The paper is organized as follows. Section 2 provides a brief background on ESNs and the level set method. Then, in Section 3, our proposed hybrid level set/ESN model is described, with a novel calibration algorithm to quantify the uncertainty. We show the forecasting performance of our proposed model through simulation experiments and real data in Section 4 and 5, respectively. Finally, Section 6 provides a brief discussion.

2 Background

This section provides brief background on ESNs and the level set method to facilitate discussion of the new model in Section 3.

2.1 Echo State Network (ESN)

The ESN has been an appealing type of recurrent neural network due to its relatively inexpensive computational cost, reduced training data burden, and conceptual simplicity (Lukoševičious, 2012). The basic vanilla ESN model for time $t = 1, \dots, T$ can be written as follows:

$$\begin{aligned}
\text{response : } \quad & \mathbf{v}_t = g_o(\mathbf{o}_t) \\
\text{output : } \quad & \mathbf{o}_t = \mathbf{W}^{out} \mathbf{h}_t \\
\text{hidden state : } \quad & \mathbf{h}_t = (1 - \alpha_\ell) \mathbf{h}_{t-1} + \alpha_\ell \tilde{\mathbf{h}}_t \\
& \tilde{\mathbf{h}}_t = g_h \left(\frac{\nu}{|\lambda_w|} \mathbf{W}^{in} \mathbf{h}_{t-1} + \mathbf{U} \mathbf{x}_t \right), \\
\text{parameters : } \quad & \mathbf{W}^{in} = [w_{i,\ell}^{in}]_{i,\ell} : \gamma_{i,\ell}^w \text{Unif}(-a_w, a_w) + (1 - \gamma_{i,\ell}^w) \delta_0 \\
& \mathbf{U} = [u_{i,j}]_{i,j} : \gamma_{i,j}^u \text{Unif}(-a_u, a_u) + (1 - \gamma_{i,j}^u) \delta_0 \\
& \gamma_{i,\ell}^w \sim \text{Bern}(\pi_w) \\
& \gamma_{i,j}^u \sim \text{Bern}(\pi_u),
\end{aligned} \tag{1}$$

where $N \times 1$ vector \mathbf{v}_t , $N \times 1$ vector \mathbf{o}_t , $J \times 1$ vector \mathbf{h}_t , and $n_u \times 1$ vector \mathbf{x}_t correspond to the response, output, hidden units, and input signal, respectively. Critically, the $J \times J$ matrix \mathbf{W}^{in} and $J \times n_u$ matrix \mathbf{U} are pre-specified weight matrices with elements drawn randomly from specified distributions with hyperparameters a_w , a_u , π_w and π_u . δ_0 is a Dirac delta function at zero. Note that hyperparameters π_w and π_u control the sparsity of the matrices \mathbf{W}^{in} and \mathbf{U} , respectively. Additionally, λ_w is the spectral radius of \mathbf{W}^{in} , $\alpha_\ell \in (0, 1]$ is the so-called ‘‘leaking rate’’, and ν is a tuning parameter. The element-wise activation functions $g_o(\cdot)$ and $g_h(\cdot)$ are user-specified, but $\tanh(\cdot)$ functions are typically chosen for $g_h(\cdot)$, an identity function is typically chosen for $g_o(\cdot)$ when the response is continuous, and a softmax functions is typically chosen for categorical responses. As discussed by Lukoševičious (2012), the role of the hidden units in an ESN is to project the inputs into a higher dimensional space through nonlinear expansion and to simultaneously remember the input.

To approximate the nonlinear system well, an ESN should exhibit the ‘‘echo state property’’ (Zhang et al., 2012), which essentially ensures that the reservoir model will eventually not be sensitive to initial conditions. This is ensured in most cases if the spectral radius of \mathbf{W}^{in} is less than 1 (Lukoševičious, 2012). The ratio of the parameter ν and the largest eigenvalue λ_w of \mathbf{W}^{in} in the hidden state control the effective spectral radius. That is, $0 < \nu < 1$ guarantees the spectral radius of the model will be less than 1.

The key to reservoir methods such as the ESN is that one only needs to estimate the $N \times J$ read-out matrix \mathbf{W}^{out} , which provides tremendous savings in terms of computational cost and the amount of data required to train the model. However, to prevent overfitting, it is very important that this estimation is regularized, which is typically accomplished using an ℓ_2 penalty (i.e., ridge regression). For illustration, one can write the loss function, assuming the identity

function for $g_o(\cdot)$, as

$$\widehat{\mathbf{W}}^{out} = \arg \min_{\mathbf{V}} \left[\frac{1}{N} \sum_{t=1}^T \left((\mathbf{v}_t - \mathbf{W}^{out} \mathbf{h}_t)^\top (\mathbf{v}_t - \mathbf{W}^{out} \mathbf{h}_t) \right) + \tau \sum_{j=1}^J \|\mathbf{w}_{:j}^{out}\|^2 \right], \quad (2)$$

where $\mathbf{w}_{:j}^{out}$ is j^{th} column in \mathbf{W}^{out} , $\tau \in (0, \infty)$ is the regularization parameter, and $\|\cdot\|$ is the ℓ_2 norm. One can easily obtain the solution for (2) in closed form (Lukoševičius, 2012).

Despite its conceptual simplicity and computational efficiency, selection of the tuning parameters in the ESN can be burdensome. Lukoševičius (2012) provides concise guidelines for the hyperparameters π_w, π_u, a_w , and a_u . In particular, they recommend sparse connections between units (i.e., small π_w and π_u) to induce sparsity in \mathbf{W}^{in} and \mathbf{U} , but recommend that \mathbf{U} be more dense than \mathbf{W}^{in} . The role of a_u and a_w is to determine the effect of input \mathbf{x}_t and previous hidden state \mathbf{h}_{t-1} on the current hidden state \mathbf{h}_t (Lukoševičius, 2012). In addition to π_w, π_u, a_w , and a_u , one must select the reservoir size J , the leakage rate α_ℓ , and the echo-state parameter ν . Selection of the hyperparameters α_ℓ and J can be accomplished by cross-validation or validation, but can be computationally inefficient. McDermott and Wikle (2017) used grid search with a validation approach for finding the best set of hyperparameters, and McDermott and Wikle (2019) used a genetic algorithm (e.g., Sivanandam and Deepa, 2008) in a “deep” ESN to accommodate the increased number of hyperparameters present in deep ESNs. Ribeiro et al. (2020) applied a Bayesian optimization algorithm to an ESN for short-term load forecasting, and Thiede and Parlitz (2019) proposed a gradient-based optimization algorithm, which was shown to be superior to grid search for large numbers of hyperparameters. A systematic review of hyperparameter optimization for ESNs can be found in Matzner (2022).

Historically, the quantification of uncertainty in neural models presents a significant challenge (e.g., see Abdar et al., 2021; Wikle and Zammit-Mangion, 2022, for general discussion). This is also true with reservoir methods. One useful approach that has been used for ESNs is to generate ensembles from the reservoir (Yao et al., 2013; Sheng et al., 2013). For example, McDermott and Wikle (2017) and McDermott and Wikle (2019) constructed forecasting ensembles by sampling the recurrent and input weight matrices independently from their reservoir distributions. In a Monte Carlo sense, the $(1-\alpha)\%$ forecasting intervals were then obtained from the element-wise percentiles of the forecasting ensembles. Bonas and Castruccio (2021) also generated ensemble forecasts on the training set and quantified the uncertainty by calibrating the residual with monotone cubic spline interpolation. In addition to the ensemble approach, McDermott and Wikle (2019) adopted stochastic search variable selection priors (George and McCulloch, 1993) for their Bayesian ESN. Atencia et al. (2020) employed Monte Carlo Dropout (Gal and Ghahramani, 2016) as another straightforward strategy, which is similar to the ensemble approaches in principle.

2.2 The Level Set Method

The level set method (or the level set equation), proposed by Osher and Sethian (1988), is an advection-diffusion equation used to model the evolution of an implicit function in an arbitrary dimension. That is,

$$\frac{\partial \phi(\mathbf{s}, t)}{\partial t} + \mathbf{v}(\mathbf{s}, t) \cdot \nabla \phi(\mathbf{s}, t) = 0, \quad (3)$$

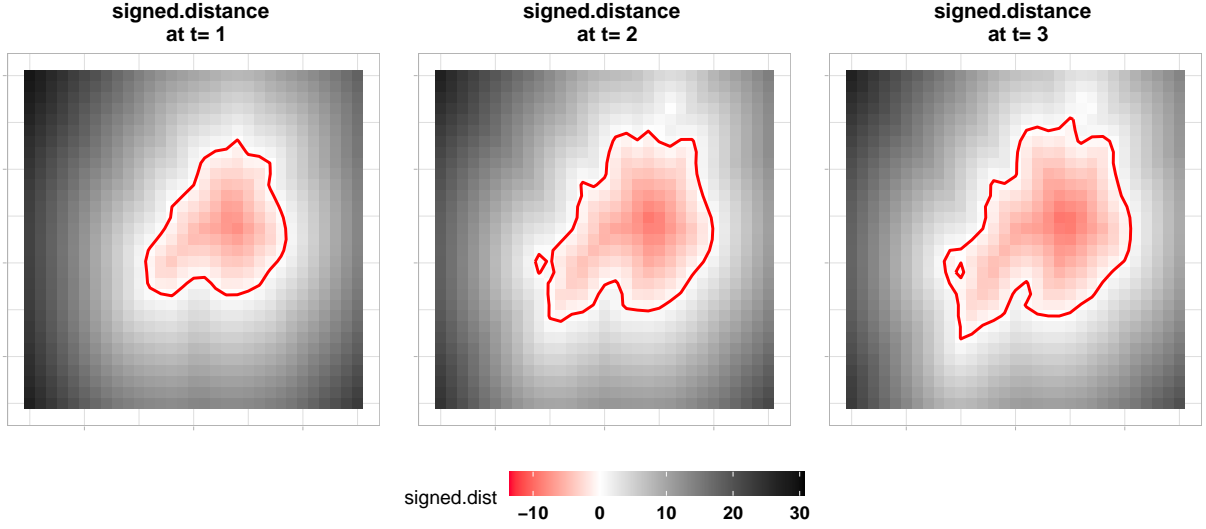


Figure 1: Illustration of a signed distance function: Three boundaries at $t = 1, 2, 3$ are depicted from the left to right.

where $\phi(\mathbf{s}, t)$ is an implicit function evaluated at location \mathbf{s} and time t , $\frac{\partial \phi(\mathbf{s}, t)}{\partial t}$ denotes the temporal partial derivative, and $\mathbf{v}(\mathbf{s}, t) = (v_x(\mathbf{s}, t), v_y(\mathbf{s}, t))^T \in \mathbb{R}^2$ is the velocity that controls the direction and speed of the implicit function evolution. By construction, the level set method requires an implicit function, leading to the Eulerian representation of the boundary in wildfire applications. In Eulerian approaches, one represents the boundary implicitly through a contour function, as opposed to Lagrangian frameworks where one defines a set of points on the boundary to describe the boundary explicitly. (Osher and Fedkiw, 2002). Eulerian representations can be computationally more expensive than Lagrangian methods, yet Eulerian approaches are typically more effective in representing complicated boundaries and their change through time; for example, when wildfires exhibit topological changes such as merging or splitting.

It is common to use a signed distance function for the implicit function in the level set method due to its straightforward interpretation and mathematical simplicity. The signed distance function $\phi(\mathbf{s})$ for $\forall \mathbf{s} \in \mathbb{R}^2$ is

$$\phi(\mathbf{s}) = \begin{cases} -d(\mathbf{s}), & \mathbf{s} \in \Omega^- \\ 0, & \mathbf{s} \in \partial\Omega \\ d(\mathbf{s}), & \mathbf{s} \in \partial\Omega^+ \end{cases}, \quad (4)$$

where Ω^- , Ω^+ , and $\partial\Omega$ are the interior, and exterior of the boundary and the boundary itself, respectively. Here, $d(\mathbf{s})$ is the closest distance from \mathbf{s} to the boundary. Assuming a distance given by the ℓ_2 norm,

$$d(\mathbf{s}) = \min(\|\mathbf{s} - \mathbf{s}_I\|), \quad (5)$$

where $\mathbf{s}_I \in \partial\Omega$ is the set of points on the boundary. For an illustration of a signed distance function evolving in time, see Figure 1. During the evolution, one can see that a new boundary appears at $t = 2$ on the bottom left, and a closed loop exists inside the main boundary at $t = 3$. Regardless of any topological change the boundary exhibits, one can represent the boundary with the set $\partial\Omega = \{\mathbf{s} : \phi(\mathbf{s}) = 0\}$. Additionally, a signed distance function has the convenient mathematical property that

$$\|\nabla\phi(\mathbf{s}, t)\| = 1, \quad (6)$$

where $\nabla\phi(\mathbf{s}, t)$ indicates a spatial gradient of $\phi(\mathbf{s}, t)$.

Notably, the frequently-made assumption that the evolution is in the normal direction to the boundary (e.g., Mallet et al., 2009; Alessandri et al., 2021; Yoo and Wikle, 2022) and (6) simplifies (3) so that

$$\frac{\partial\phi(\mathbf{s}, t)}{\partial t} + v_n(\mathbf{s}, t) = 0, \quad (7)$$

where $v_n(\mathbf{s}, t)$ is the scalar velocity (speed) in the normal direction. (7) can then be simply approximated by a forward Euler discretization

$$\frac{\phi(\mathbf{s}, t + \Delta t) - \phi(\mathbf{s}, t)}{\Delta t} + v_n(\mathbf{s}, t) = 0, \quad (8)$$

where Δt is time-step size. Although one can still solve (3) without assumption (6) with numerical solvers (Osher and Fedkiw, 2002), it induces more computational cost. Importantly, there is not much to be gained by such complexity in data-driven approaches so long as one can learn the spatial and temporally varying speed in the normal direction, $v_n(\mathbf{s}, t)$. Indeed, as discussed in Section 1, it is crucial in wildfire applications to estimate this to obtain realistic fire boundary propagation in complex fires. Building on the flexibility and convenience of the ESN, Section 3 presents a novel model that embeds an ESN within the level set equation to estimate $v_n(\mathbf{s}, t)$ in (8).

3 Hybrid Level Set/ESN Model

This section presents a model in which an ESN, used to learn propagation speed, is embedded within the level set method. Section 3.1 illustrates the structure of the model. Section 3.2, 3.3, and 3.4 present the hyperparameter tuning approach, uncertainty quantification method, tuning selection, and the algorithm, respectively.

3.1 Nested ESN Model

The hybrid level set/ESN model considers a vectorized form of equation (8) with additive error in which the spatio-temporal speeds in the normal direction to the boundary are specified via an ESN. Specifically, for spatial locations

$\mathbf{s}_i, 1 \leq i \leq N$ in the domain of interest $\mathcal{D} \subset \mathbb{R}^2$ and time indexed by $t, 1 \leq t \leq T$, the full model is given by:

$$\begin{aligned}
\text{response : } \quad & \phi_t = \phi_{t-\Delta t} - \mathbf{v}_{n,t-\Delta t} \Delta t + \boldsymbol{\epsilon}_t \\
\text{rate of spread : } \quad & \mathbf{v}_{n,t-\Delta t} = \mathbf{W}^{out} \mathbf{h}_{t-\Delta t} \\
\text{hidden state : } \quad & \mathbf{h}_{t-\Delta t} = (1 - \alpha_\ell) \mathbf{h}_{t-2\Delta t} + \alpha_\ell \tilde{\mathbf{h}}_{t-\Delta t} \\
& \tilde{\mathbf{h}}_{t-\Delta t} = g_h \left(\frac{\nu}{|\lambda_w|} \mathbf{W}^{in} \mathbf{h}_{t-2\Delta t} + \mathbf{U} \mathbf{x}_{t-\Delta t} \right) \\
\text{parameters : } \quad & \mathbf{W}^{in} = [w_{i,\ell}^{in}]_{i,\ell} : \gamma_{i,\ell}^w \text{Unif}(-a_w, a_w) + (1 - \gamma_{i,\ell}^w) \delta_0 \\
& \mathbf{U} = [u_{i,j}]_{i,j} : \gamma_{i,j}^u \text{Unif}(-a_u, a_u) + (1 - \gamma_{i,j}^u) \delta_0 \\
& \gamma_{i,\ell}^w \sim \text{Bern}(\pi_w) \\
& \gamma_{i,j}^u \sim \text{Bern}(\pi_u),
\end{aligned} \tag{9}$$

where $\phi_t = (\phi(\mathbf{s}_1, t), \dots, \phi(\mathbf{s}_N, t))^\top$, $\mathbf{v}_{n,t-\Delta t} = (v_n(\mathbf{s}_1, t - \Delta t), \dots, v_n(\mathbf{s}_N, t - \Delta t))^\top$, and $\boldsymbol{\epsilon}_t = (\epsilon(\mathbf{s}_1, t), \dots, \epsilon(\mathbf{s}_N, t))^\top$ denote an observed signed distance function, rate of spread in the normal direction to the boundary, and error term on the space \mathcal{D} at the indexed time, respectively. Note that rate of spread (speed), hidden state, and parameters model are equivalently defined as in (1).

The nested ESN model used to estimate the rate of spread $\mathbf{v}_{n,t-\Delta t}$ can provide more data-driven learning flexibility than the linear formulation in [Yoo and Wikle \(2022\)](#) and the Rothermel model ([Rothermel, 1972](#)). Importantly, one only needs to estimate the read-out matrix \mathbf{W}^{out} after the appropriate hyperparameters are specified. If ridge regression is used as in (2), one also must specify the penalty coefficient τ , but this is still computationally efficient.

As indicated in Section 2, uncertainty quantification and the selection of hyperparameters in this model must be accounted for. We quantify forecast uncertainty through ensembles, but our method is motivated by the highest density region proposed by [Hyndman \(1996\)](#) and calibration strategy of [Daw and Wikle \(2022\)](#) as described in Section 3.2. We adopt a random search approach for hyperparameter tuning ([Bergstra and Bengio, 2012](#)) as described in Section 3.3. The complete algorithm for our hybrid models is presented in Section 3.4.

3.2 Uncertainty Quantification

Once the model is fitted, a one-step ahead forecast for time $T + 1$ is given by

$$\hat{\phi}_{T+1} = \phi_T - \widehat{\mathbf{W}}^{out} \mathbf{h}_T \Delta t, \tag{10}$$

where \mathbf{h}_T is obtained from (9) given \mathbf{W}^{in} , \mathbf{U} , α_ℓ , J and ν . To quantify the uncertainty associated with this forecast, we take the ensemble approach motivated by [Sheng et al. \(2013\)](#), [Yao et al. \(2013\)](#), and [McDermott and Wikle \(2017\)](#). That is, we collect an ensemble of $N_{ensemble}$ forecasts $\hat{\phi}_{en,T+1} = (\hat{\phi}_{T+1}^{(1)}, \dots, \hat{\phi}_{T+1}^{(N_{ensemble})})$ where each forecast is associated with different hyperparameters and reservoir matrices. We then construct $(1 - \alpha)\%$ forecast intervals at

location \mathbf{s} as

$$\left(\hat{\ell}_{T+1}(\mathbf{s}), \hat{u}_{T+1}(\mathbf{s})\right) = \underset{\ell_{T+1}(\mathbf{s}), u_{T+1}(\mathbf{s})}{\arg \min} \left(u_{T+1}(\mathbf{s}) - \ell_{T+1}(\mathbf{s})\right) \quad (11)$$

such that

$$\frac{1}{N_{ensemble}} \sum_{i=1}^{N_{ensemble}} I\left(\ell_{T+1}(\mathbf{s}) \leq \hat{\phi}_{T+1}^{(i)}(\mathbf{s}) \leq u_{T+1}(\mathbf{s})\right) = 1 - \alpha, \quad (12)$$

where $\ell_{T+1}(\mathbf{s})$ and $u_{T+1}(\mathbf{s})$ are the interval lower and upper bounds.

The motivation for (12) is from the calibration strategy of [Daw and Wikle \(2022\)](#). To quantify the uncertainty for spatial prediction in reservoir models, [Daw and Wikle \(2022\)](#) first obtained the median and inter-quartile range from ensembles and trained the optimal calibration cutoff value to ensure a $(1 - \alpha)\%$ coverage rate over the training set. Then, the prediction intervals for their test set were constructed from the median and interquartile range from the ensembles over the test set and the cutoff value obtained from the training set. Here, we do not require a separate training set calibration because the coverage rate is given directly in (12) based on ensembles of forecasts.

The highest density region proposed by [Hyndman \(1996\)](#) motivates the relationship in (11). The highest density region provides the shortest intervals, which may consist of several disjoint intervals for multimodal distributions ([Hyndman, 1996](#)). However, several disjoint intervals complicate the interpretation in wildfire applications, which leads to quantifying the uncertainty by single intervals as given in (11). The aim of using the $(1-\alpha)\%$ highest density intervals is to exclude the poor forecasts (e.g., outliers), which we find effective in our simulation experiments and real data analysis.

3.3 Hyperparameter tuning

Hyperparameter selection is one of the most important components when building deep neural models ([Probst et al., 2018](#)). The most intuitive and straightforward approach is to use a grid search to explore the parameter space. However, such methods are inefficient for relatively high-dimensional parameter spaces. An efficient alternative is to use random search (e.g., [Bergstra and Bengio, 2012](#)), which improves on grid search by randomly searching over hyperparameters from specified ‘‘prior’’ distributions ([Yu and Zhu, 2020](#)), and can be implemented at a fraction of the cost of optimization algorithms. For an extensive review of hyperparameter optimization strategies, refer to [Yu and Zhu \(2020\)](#).

We use a version of random search for our hybrid level set/ESN algorithm. The ensemble approach to ESN modeling allows one to not only sample from the reservoirs for each ensemble member, but also the hyperparameter distributions. Specifically, we draw a_u, a_w, J, τ, ν , and α_ℓ for each ensemble member independently from their prior distributions. The guidelines from [Lukoševičious \(2012\)](#) can help determine fixed values for π_w, π_u , and the distributions from which hyperparameters are drawn. It is important to note that significant computational efficiency is gained from

selecting the hyperparameters through random search, and also provides uncertainty quantification as described in Section 3.2.

3.4 Hybrid level set/ESN algorithm

Algorithm 1 Hybrid Level Set/ESN Algorithm

- 1: **Input** Data $\{\phi_t\}$ for $t = 1, \dots, T$. The prior distributions of a_u, a_w, J, τ, ν , and α_ℓ denoted by $P(a_u), P(a_w), P(J), P(\tau), P(\nu), P(\alpha_\ell)$, respectively. Fixed constants π_w and π_u .
 - 2: **for** $k = 1 : N_{ensemble}$ **do**
 - 3: Randomly draw $a_u^{(k)}, a_w^{(k)}, J^{(k)}, \tau^{(k)}, \nu^{(k)}$, and $\alpha_\ell^{(k)}$ from prior distributions.
 - 4: Construct $\mathbf{W}^{in,(k)}, \mathbf{U}^{(k)}$ with sampled $a_w^{(k)}, a_u^{(k)}, \nu^{(k)}, \pi_w$, and π_u .
 - 5: Fit the model in (9) with $J^{(k)}$ and $\alpha_\ell^{(k)}$, and estimate $\widehat{\mathbf{W}}^{out,(k)}$ by ridge regression with $\lambda^{(k)}$.
 - 6: Obtain the forecasts $\widehat{\phi}_{T+1}^{(k)}$ using $\widehat{\mathbf{W}}^{out,(k)}$.
 - 7: **end for**
 - 8: Define the ensemble of forecasts: $\widehat{\phi}_{en,T+1} = \{\widehat{\phi}_{T+1}^{(1)}, \dots, \widehat{\phi}_{T+1}^{(N_{ensemble})}\}$
 - 9: Ensemble forecast median: $\widehat{\phi}_{med,T+1} = \text{median}(\widehat{\phi}_{en,T+1})$
 - 10: Ensemble uncertainty: $(\widehat{\ell}_{T+1}, \widehat{u}_{T+1})$ obtained by (11) and (12) corresponding to the significance level α .
 - 11: **output** $\widehat{\phi}_{med,t+1}$ and $(\widehat{\ell}_{T+1}, \widehat{u}_{T+1})$
-

The hybrid level set/ESN model, including the uncertainty quantification and hyperparameter selection described in Section 3.2 and 3.3, is detailed in Algorithm 1.

Step 3 of Algorithm 1 draws hyperparameters $a_u^{(k)}, a_w^{(k)}, J^{(k)}, \tau^{(k)}, \nu^{(k)}$, and $\alpha_\ell^{(k)}$ from their prior distributions (i.e., random search), from which recurrent and input weight matrices $\mathbf{W}^{in,(k)}$ and $\mathbf{U}^{(k)}$ are constructed in Step 4. Fitting model (9) and estimating $\widehat{\mathbf{W}}^{out,(k)}$ with $\tau^{(k)}$ is conducted in Step 5, and Step 6 produces forecast ensemble members

$$\widehat{\phi}_{T+1}^{(k)} = \phi_T - \widehat{\mathbf{W}}^{out,(k)} \mathbf{h}_T^{(k)} \Delta t, \quad (13)$$

where $\mathbf{h}_T^{(k)}$ is constructed by (9) with $\mathbf{W}^{in,(k)}, \mathbf{U}^{(k)}, \alpha_\ell^{(k)}, J^{(k)}$ and $\nu^{(k)}$. After $N_{ensemble}$ iterations of Steps 3 to 6, which creates the ensembles $\widehat{\phi}_{en,T+1} = (\widehat{\phi}_{T+1}^{(1)}, \dots, \widehat{\phi}_{T+1}^{(N_{ensemble})})$, Algorithm 1 provides the median of $\widehat{\phi}_{en,T+1}$ for the point forecast estimate and quantifies the uncertainty with $(1 - \alpha)\%$ intervals of $\widehat{\phi}_{en,T+1}$ using (11) and (12).

We show the forecasting performance of this algorithm through simulation experiments and with wildfire data in Sections 4 and 5, respectively.

4 Simulation experiments

To make simulations more realistic, we generate two datasets by evolving a randomly generated initial closed boundary with the actual wind speeds obtained from the R package *rWind* (Fernández-López, 2022). Specifically, we first obtain twenty series of wind speeds from 2018-06-25 00:00:00 to 2018-07-04 12:00:00 at every twelve hours over longitude and latitude $[90,150] \times [5,40]$. Then, the initial closed boundary is evolved from these wind speeds using equation 8. The first generated dataset (see the left panel in Figure 2) exhibits an evolution that includes disjoint boundaries merging into one. The second dataset (see the right panel of Figure 2) is generated with topological constraints, similar

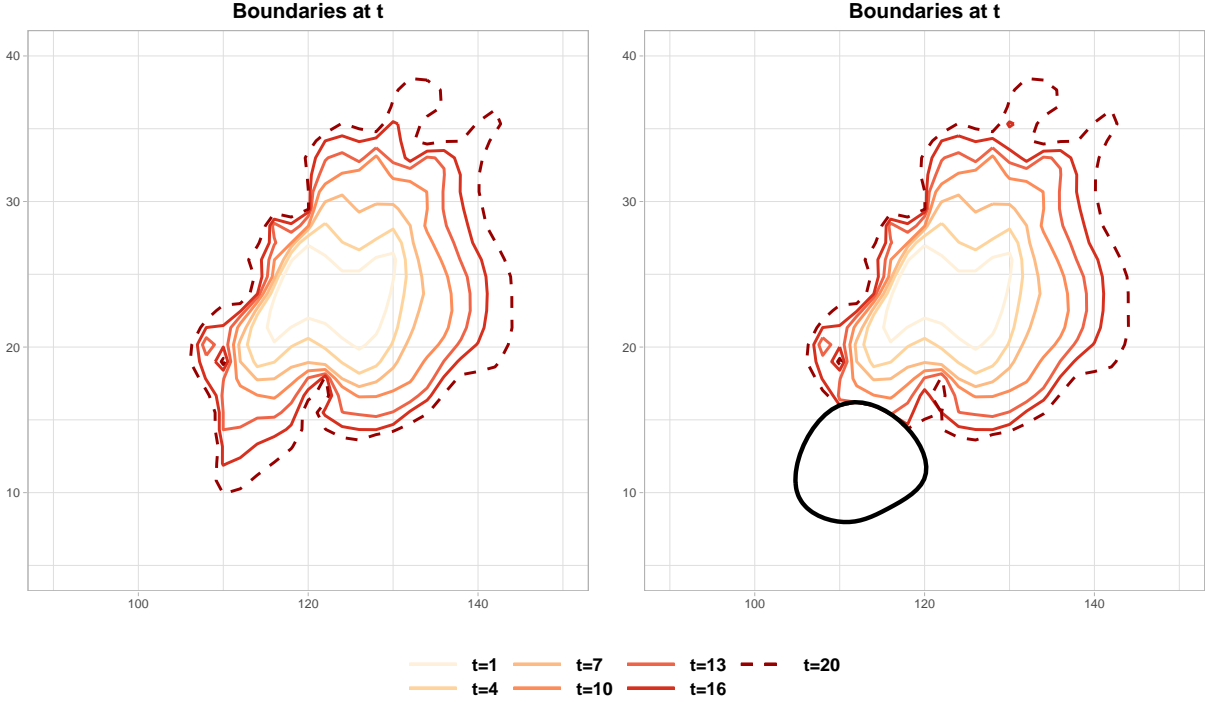


Figure 2: Simulation experiments: the evolution of boundaries for each simulation. In the left figure, the evolution to the northeast is prominent. In the right figure, evolution is equivalent to the first simulation, but constraint (solid black line) prevents the spread over it.

to a spatial area that might prevent wildfire spread (e.g., rivers, lakes, or oceans). Topological constraints are depicted in a solid black line for the second dataset. On both figures, the dashed line indicates the boundary we seek to forecast.

We first obtain a signed distance function on a 31×31 grid on the domain $[90, 150] \times [5, 40]$. Then, we leave out data at $t = 20$ to evaluate forecasting performance. That is, we fit our proposed model (9) on data from $t = 1, \dots, 19$ and obtain a one-step ahead forecast at $t = 20$ by Algorithm 1 with $\Delta t = 0.1$. For the hyperparameter distributions, we set $P(a_u) = P(a_w) = (0.1, 0.5, 1)$, $P(\alpha_\ell) = (0.01, 0.0621, \dots, 0.9478, 1)$, $P(\nu) = (0.1, 0.2, \dots, 0.8, 0.9)$, $P(\tau) = (0.001, 1.112, \dots, 8.889, 10)$, and $P(J) = (50, \dots, 100)$. The values of $P(J)$ are relatively small to prevent overfitting, so each ensemble member functions as a relatively weak learner (McDermott and Wikle, 2017). Finally, we fix $\pi_w = 0.3$ and $\pi_u = 0.5$ based on the guidelines in Lukoševičius (2012).

The choice of input is application-specific. McDermott and Wikle (2017) used embeddings (lagged values of the data) for the input \mathbf{x}_t , which we follow. Specifically, we set

$$\mathbf{x}_t = [\phi_t^\top, \phi_{t-\Delta t}^\top]^\top. \quad (14)$$

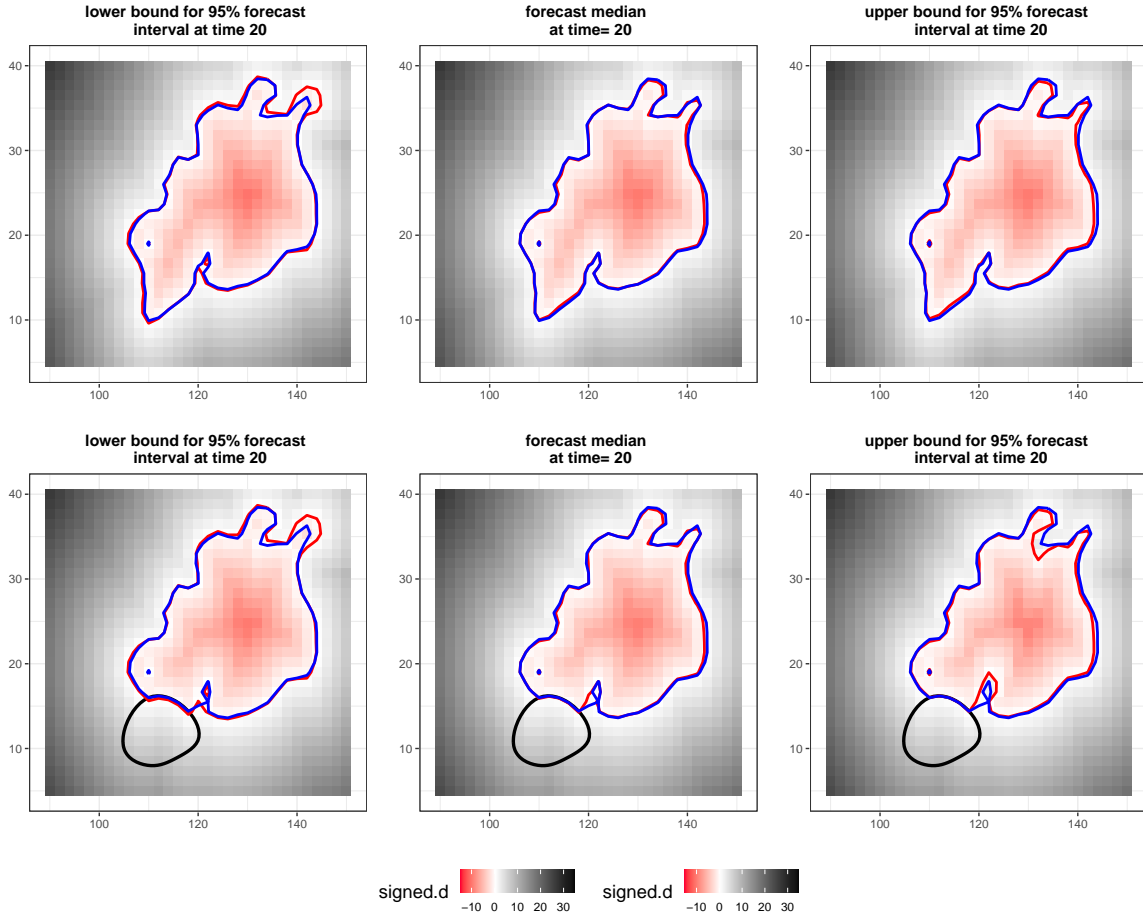


Figure 3: Simulation experiments: 95% forecast intervals and forecast median. Figures in the first and second rows correspond to the first and second simulations. The solid blue line denotes the true boundary, and the solid red line indicates the predicted boundary.

Embeddings are motivated by a nonlinear Hamilton-Jacobi equation in the level set method. Namely, the level set method in (7) becomes a nonlinear Hamilton-Jacobi equation if $v_n(s, t)$ depends on $\phi(s, t)$ (Osher and Sethian, 1988), which occurs in the ESN if we consider embeddings as in (14). Finally, we set the initial value of the hidden state $\mathbf{h}_1 = \mathbf{U} \times \mathbf{x}_{1+\Delta t} = \mathbf{U} \times [\phi_{1+\Delta t}^\top, \phi_1^\top]^\top$.

Figure 3 shows the 95% forecast intervals and median from 3,000 ensembles. One can see that the 95% forecast intervals are quite narrow, but they mainly capture the true boundary. The northeast part of the boundary shows the most variability, which aligns with the evolution pattern depicted in Figure 2. Moreover, the 95% forecast intervals for the second simulation account for the topological constraints (although the predicted boundary spreads very slightly over the topological constraints in the lower bound).

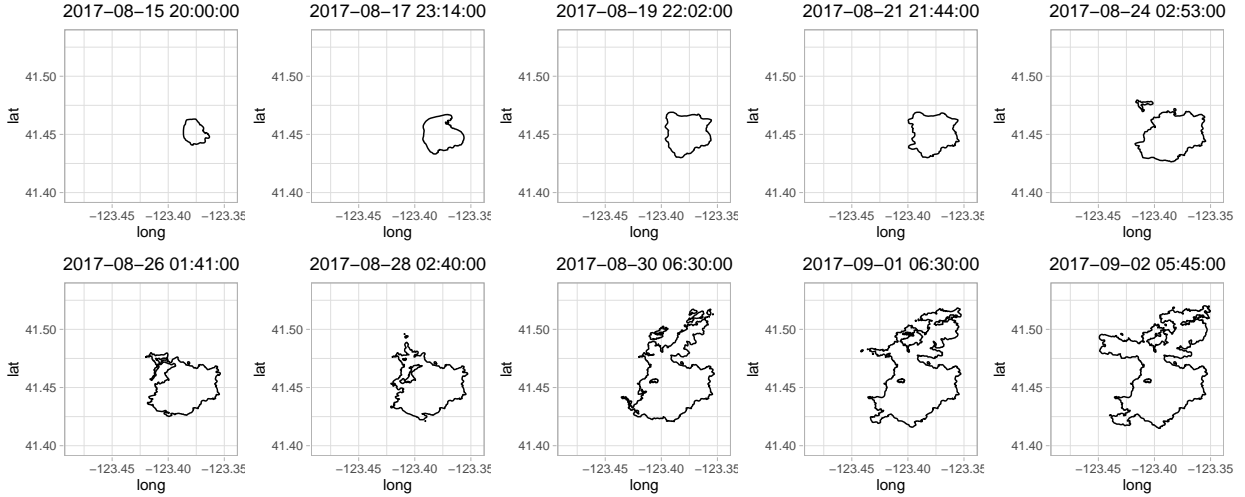


Figure 4: Fire boundaries for various times during the Haypress fire. Although the rate of spread was relatively slow until 2017-18-28 02:40:00, it subsequently accelerated, especially to the west at 2017-09-02 05:45:00.

We adopt the threat score (TS) as a summary measure (e.g., [Wikle et al. \(2019\)](#)) to assess the quality of the forecast median. Specifically, the TS is defined as

$$TS = \frac{A_{11}}{A_{11} + A_{10} + A_{01}}, \quad (15)$$

where A_{11} is the common area where the model predicts an event that eventually occurs, A_{10} is the area where the model expects an event to occur but not eventually occur, and A_{01} is the area where an event occurs, but the model fails to predict its occurrence. The range of TS summary measure is from 0 to 1, where a value of 1 indicates a perfect forecast. For a continuous variable such as a signed distance function, one needs a threshold parameter τ to determine the occurrence of an event. Therefore, we set $\tau = 0$ since points on the boundary have a signed distance of 0. That is, if $\phi(\mathbf{s}, t) \leq 0$, we consider that an event occurred on \mathbf{s} at t . The TS summary measures for the forecast median of the first and second simulations are 0.969 and 0.963, demonstrating that our model provides good forecasting performance.

5 Wildfire applications

In this section we investigate the forecasting performance of our model on two real datasets - the Haypress and Thomas megafires that occurred in California in 2017.

5.1 The Haypress fire

The Haypress fire, ignited in July 2017 and was contained in January 2018. It was the largest wildfire among the Orleans Complex fires, which burned over 27,000 acres in Siskiyou County, California. We consider the first 11 observations of the Haypress fire boundary from GeoMac database ([Geospatial Multi-Agency Coordination Group, 2019](#))

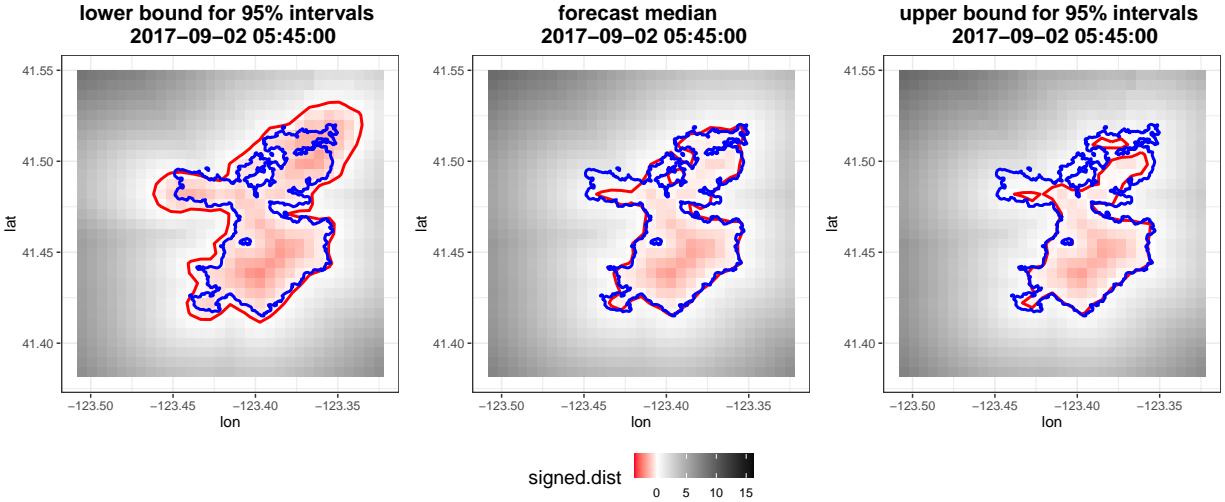


Figure 5: Forecast medians and 95% intervals for the Haypress fire. The solid blue lines denote the true boundary, while the solid red lines indicates the predicted boundary. Most of the variability in forecast intervals is observed on the left part of the boundary.

for this analysis. Specifically, we fit the model (9) on the first ten observations, leaving out the eleventh observation to evaluate forecasting performance. Figure 4 shows the wildfire propagation from the second observation to the eleventh observation, from which one can see the rapid rate of spread to the north at 2017-08-30 06:30:00 and to the west at 2017-09-02 05:45:00. The forecasting task is more challenging than the simulation experiments in that a predominant expansion to the west shown at 2017-09-02 05:45:00 is not observed from 2017-08-13 23:32:00 to 2017-09-01 06:30:00. At 2017-09-01 06:30:00, the Haypress fire shows a slight spread to the west, but it is not as striking as observed in the boundary at 2017-09-02 05:45:00.

With a signed distance function on a 31×31 grid over $[-123.5053, -123.3252] \times [41.3840, 41.5471]$ by (4), we use Algorithm 1 to fit the model (9) with the same hyperparameter distributions and $\Delta t = 0.1$ as in the simulation experiments. Also, the inputs and initial value of the hidden state are chosen in the same manner. Figure 5 shows the 95% forecast intervals and median from 3,000 ensembles. The forecast median captures the evolution to the west, and the 95% intervals provide good coverage of the true boundary. Given the small number of observations used to train the model, the model visually shows very good forecasting performance.

Table 1: Comparison of Interval Score (IS) and Threat Score (TS) between models. \mathcal{M}_1 and \mathcal{M}_2 refer to the model presented here and the model by [Yoo and Wikle \(2022\)](#), respectively.

Model	The Haypress fire		The Thomas fire	
	Interval Score	Threat Score	Interval Score	Threat Score
\mathcal{M}_1	0.776	0.849	4.901	0.964
\mathcal{M}_2	1.730	0.791	5.286	0.954

To more objectively compare the forecast performance of our model to that by [Yoo and Wikle \(2022\)](#), we measure the quality of forecast intervals using the interval score (IS) ([Gneiting and Raftery, 2012](#)), which is given by

$$\begin{aligned}
 S_{\alpha}^{Int}(\ell(\mathbf{s}, t), u(\mathbf{s}, t), \phi(\mathbf{s}, t)) = & \\
 & (u(\mathbf{s}, t) - \ell(\mathbf{s}, t)) + \frac{2}{\alpha}(\ell(\mathbf{s}, t) - \phi(\mathbf{s}, t))I(\phi(\mathbf{s}, t) < \ell(\mathbf{s}, t)) \\
 & + \frac{2}{\alpha}(\phi(\mathbf{s}, t) - u(\mathbf{s}, t))I(\phi(\mathbf{s}, t) > u(\mathbf{s}, t)),
 \end{aligned} \tag{16}$$

where $\ell(\mathbf{s}, t)$, $u(\mathbf{s}, t)$, α , and $\phi(\mathbf{s}, t)$ are the lower bound, upper bound, significance level, and true signed distance function on \mathbf{s} at t . The IS consists of the length of an interval ($u(\mathbf{s}, t) - \ell(\mathbf{s}, t)$) and the penalty ($\frac{2}{\alpha}(\ell(\mathbf{s}, t) - \phi(\mathbf{s}, t))$ or $\frac{2}{\alpha}(\phi(\mathbf{s}, t) - u(\mathbf{s}, t))$) induced if forecast intervals fail to contain $\phi(\mathbf{s}, t)$. A smaller IS indicates better forecast intervals. The IS is intuitively appealing since it favors narrow forecast intervals but penalizes if those are too narrow. Furthermore, the IS is a proper scoring rule ([Gneiting and Raftery, 2012](#)). We summarize the quality of forecasting intervals by

$$IS = \frac{\sum_{\mathbf{s}: \phi(\mathbf{s}, t) \leq 0} S_{\alpha}^{Int}(\ell(\mathbf{s}, t), u(\mathbf{s}, t), \phi(\mathbf{s}, t))}{|\{\mathbf{s} : \phi(\mathbf{s}, t) \leq 0\}|}, \tag{17}$$

where $|\cdot|$ denotes the cardinality of the set and $t=2017-09-02\ 05:45:00$ for the Haypress fire. We only consider the locations inside the true boundary at 2017-09-02 05:45:00 since our primary interest is the boundary (indirectly, the burned and burning area), not the whole domain.

As given in Table 1, the TS summary measure and IS from model applied to the Haypress fire forecast are 0.849 and 0.776, respectively, while those from [Yoo and Wikle \(2022\)](#) are 0.791 and 1.730, demonstrating better forecast performance of the hybrid level set/ESN model. We also note that the computational cost of the hybrid level set/ESN is much lower than [Yoo and Wikle \(2022\)](#). Specifically, the algorithm presented in this paper takes less than 3 minutes on a standard laptop computer compared to 3 hours for the model in [Yoo and Wikle \(2022\)](#) on a high-performance cluster.

5.2 The Thomas fire

The massive Thomas fire in Southern California burned 114,000 hectares from the time of its ignition on December 4, 2017 to its containment in January 2018. Even after containment, post-fire debris flow continued to present hazards ([Addison and Oommen, 2020](#)). We consider 21 observations of fire boundaries from the GeoMac database ([Geospatial Multi-Agency Coordination Group, 2019](#)) as depicted in Figure 6. Notably, the spread rate is relatively

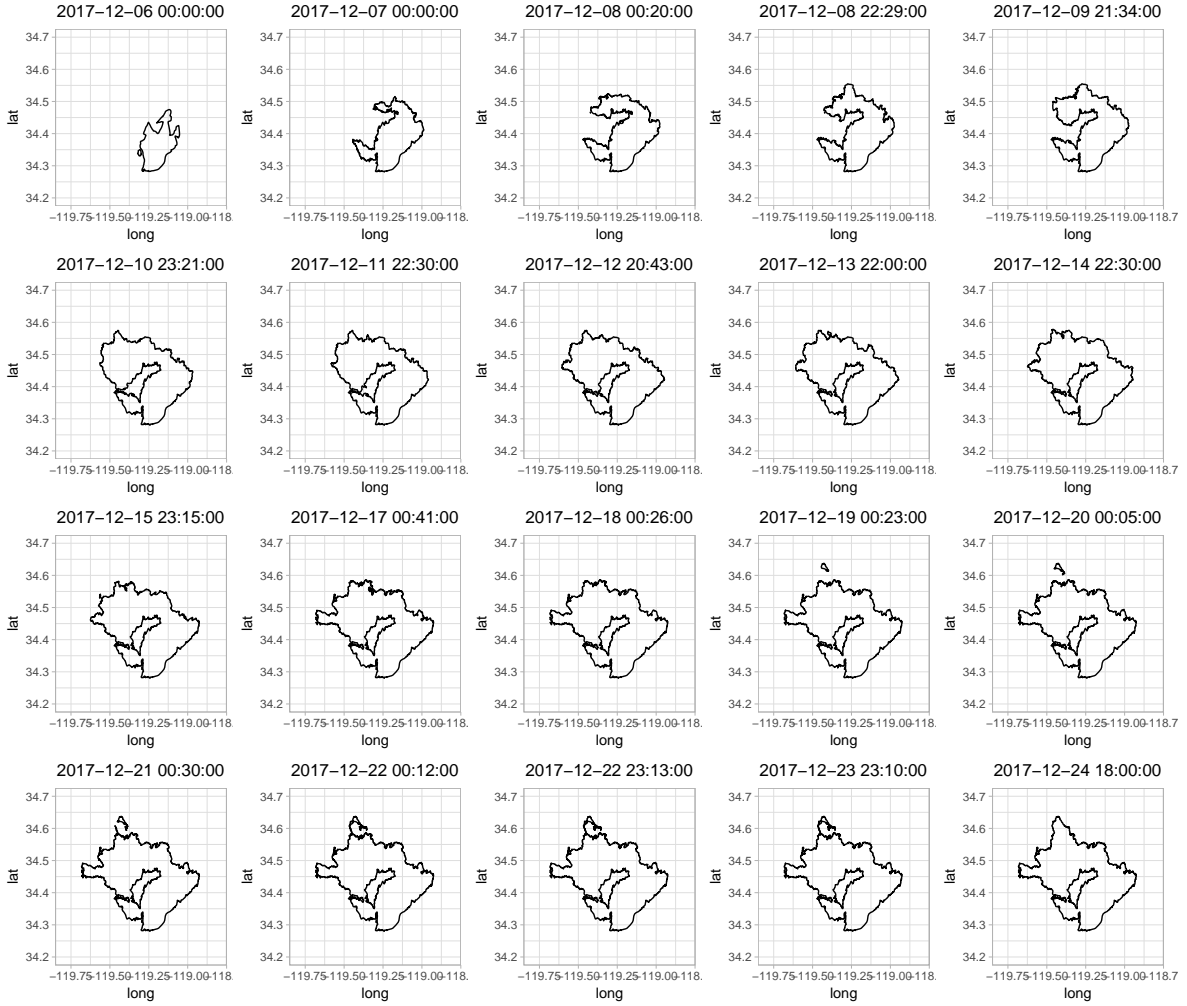


Figure 6: Thomas fire boundaries for 20 times Thomas fire (note, the first observation at 2017-12-05 04:40:00 is omitted). Compared to the Haypress fire, the rate of spread is relatively consistent in general.

more uniform than the Haypress fire, especially after 2017-12-10 23:21:00. However, there was a sudden extension of the boundary at 2017-12-24 18:00:00. This makes forecasting at 2017-12-24 18:00:00 challenging as the boundaries between 2017-12-19 00:23:00 and 2017-12-23 23:10:00 were evolving quite slowly.

We use the first twenty observations to fit the model and evaluate forecast performance at 2017-12-24 18:00:00. A signed distance function is constructed on a 30×30 grid over $[-119.8, -118.8] \times [34.2, 34.7]$ by (4). Using the same hyperparameter distributions, inputs, $\Delta t = 0.1$, and initial value of the hidden state as the simulation experiments, we obtain the forecast median and 95% forecast intervals from 3,000 ensembles, as shown in Figure 7. The forecast median fails to predict the upper part of the boundary connected at 2017-12-24 18:00:00, but importantly, the 95% forecast intervals capture this feature with a loop in the lower bound. This is a significant benefit of uncertainty quantification approach presented here.

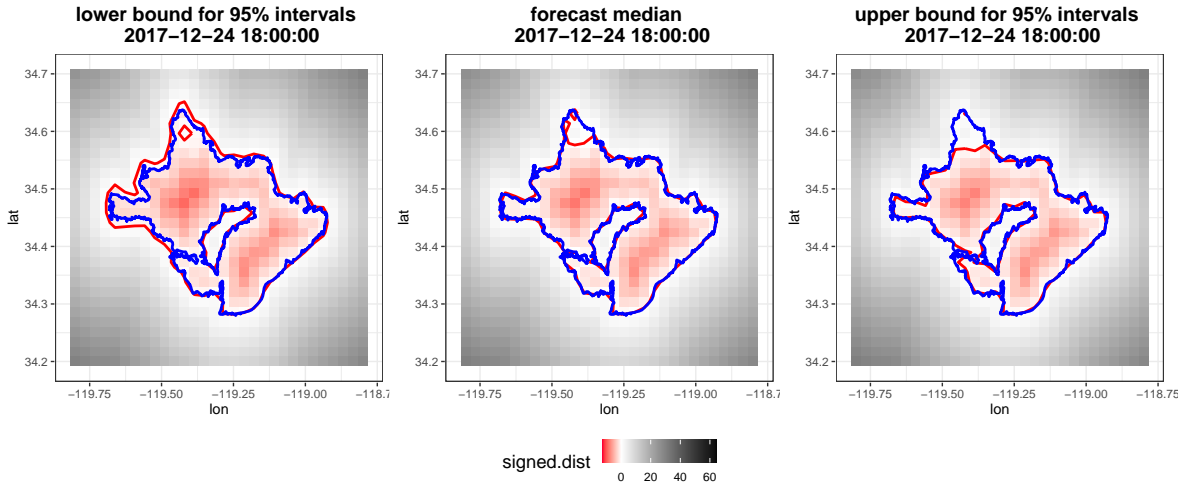


Figure 7: Forecast median and 95% intervals for the Thomas fire. The solid blue line denotes the true boundary and the solid red line indicates predicted boundary

We also compare objectively the hybrid level set/ESN model to the approach in [Yoo and Wikle \(2022\)](#) with the TS summary measure and IS. As given in Table 1, the hybrid model gives TS and IS values of 0.964 and 4.901, respectively, while [Yoo and Wikle \(2022\)](#) gave 0.954 and 5.286. These summary measures demonstrate superiority of the hybrid model, but the difference is not as dramatic as with the Haypress fire. In addition, we observe visually that the 95% credible intervals from [Yoo and Wikle \(2022\)](#) cover the true boundary without a closed loop in the lower bound, which is found in Figure 7. Nevertheless, the wider credible intervals by [Yoo and Wikle \(2022\)](#) have more negative impacts on the IS than the penalty induced by not fully covering the true boundary in the hybrid model.

6 Discussion

Although the level set method with a signed distance function has become a powerful tool in wildfire applications, the importance of data-driven learning is often neglected. Given the inhomogeneous environmental conditions and rapid spread of wildfires, it is important that the forecasting model adapt through data-driven learning. In addition, an important aspect of a trustworthy forecasting model is realistic uncertainty quantification, which is not available with deterministic model applications. Finally, a real-world wildfire forecasting model should account for nonlinearity in the fire evolution to accommodate more realistic dynamics.

We formulate our model by combining the mechanistically-motivated dynamic model (the level set method) with reservoir modeling of fire front propagation speed (ESN). Importantly, this model allows for data-driven learning as well as accounting for nonlinearity. Also, our algorithm is highly efficient and provides realistic forecasting intervals without requiring significant training costs and large amounts of data. Through simulation experiments, we demonstrate

outstanding forecasting performance. We also show that our model can provide better forecasting intervals than a state-of-the-art Bayesian level set model (Yoo and Wikle, 2022) on the Haypress and Thomas fire.

Note that we used the same distributions for hyperparameters for the simulations and real-world examples. Although for certain applications one might need to choose different distributions depending on the scale of data, our proposed random search algorithm is computationally efficient and relieves much of the burden in the tuning parameter selection as well as providing realistic forecasting intervals. Also, note that the same time-step size Δt is used for both numerical experiments and wildfire applications. We observed that the results are not very sensitive to the choice of Δt as the estimated readout matrix $\widehat{\mathbf{W}}^{out}$ adjusts to different values of Δt . Note, however, that our hybrid level set model is not limited to wildfire applications. The methodology presented here can also be used to infer shrinking boundaries, such as the response to a tumor after treatment, or the retreat of Antarctic glaciers. The key is the data-driven estimation of the speed in the normal direction to the boundary, which can easily accommodate expansion or contraction (or both in different parts of the domain).

Our model shows superior results and is more computational efficient compared to Yoo and Wikle (2022), but this does not necessarily mean that our model is more advantageous than Yoo and Wikle (2022) in every respect. Specifically, one limitation of our model is the failure to explicitly determine the effects of covariates (e.g., slope and landcover). Note that covariates, such as slope, aspect, existing vegetation cover, and forest canopy cover, can be incorporated in \mathbf{h}_1 as:

$$\mathbf{h}_1 = \mathbf{U}\mathbf{x}_{1+\Delta t} + \mathbf{U}_2\mathbf{z}_{slp} + \mathbf{U}_3\mathbf{z}_{asp} + \mathbf{U}_4\mathbf{z}_{veg} + \mathbf{U}_5\mathbf{z}_{cnp}, \quad (18)$$

where $\mathbf{Z} = [\mathbf{z}_{slp}, \mathbf{z}_{asp}, \mathbf{z}_{veg}, \mathbf{z}_{cnp}]$ denote covariates for slope, aspect, existing vegetation cover, and forecast canopy cover, while $\mathbf{U}_2, \mathbf{U}_3, \mathbf{U}_4, \mathbf{U}_5$ are pre-specified (random) weight matrices. When considering such a model, we did not observe significant improvement in forecasting with (18) and one cannot perform inference on the importance of these effects directly, as is possible in the fully hierarchical Bayesian framework in Yoo and Wikle (2022). Alternatively, one can add an additional stage in (9) to concatenate covariates in hidden states as:

$$\mathbf{h}_{t-\Delta t}^* = [\mathbf{h}_{t-\Delta t}^\top, \mathbf{z}^\top]^\top, \quad (19)$$

where $\mathbf{z}^\top = [\mathbf{z}_{slp}^\top, \mathbf{z}_{asp}^\top, \mathbf{z}_{veg}^\top, \mathbf{z}_{cnp}^\top]^\top$. Even though the readout matrix corresponding to (19) can quantify the element-wise effect of covariates, this model did not show significant improvement in forecasting. Therefore, a subject of future research is to consider alternative approaches for introducing covariates into our hybrid model in a manner that can provide explainability regarding covariate importance (e.g., Wikle et al., 2022).

Another direction in which to extend our model is to account for topological constraints explicitly. Although we demonstrate in Figure 3 that our model effectively accounts for such constraints implicitly when there is data to inform the normal speed, in situations where there are data gaps in time, or multiple time step forecasts are of interest, then explicit constraints would be important to produce realistic forecasts (e.g., accounting for water bodies). Employing

a re-initialization technique in the model could be another path. Osher and Sethian (1988) suggested occasional re-initialization to maintain a signed distance function. Nevertheless, we observe that re-initialization is not necessary for one-step ahead forecasting given data at each time step (see Figure 3, 5, and 7). Yet, for multiple-step ahead forecasting, re-initialization would likely be beneficial.

Lastly, it would be instructive to combine the level set method with other variants of ESNs. Our model is based on the basic ESN, but we could also consider quadratic or deep ESNs (e.g., McDermott and Wikle, 2017, 2019).

References

- Abdar, M., Pourpanah, F., Hussain, S., Rezazadegan, D., Liu, L., Ghavamzadeh, M., Fieguth, P., Cao, X., Khosravi, A., Acharya, U., Makarenkov, V., and Nahavandi, S. (2021). A review of uncertainty quantification in deep learning: Techniques, applications and challenges. *Information Fusion*, pages 243–297. <https://doi.org/10.1016/j.inffus.2021.05.008>.
- Addison, P. and Oommen, T. (2020). Post-fire debris flow modeling analyses: case study of the post-thomas fire event in california. *Natural Hazards*, 100:329–343. <https://doi.org/10.1007/s11069-019-03814-x>.
- Alessandri, A., Bagnerini, P., Gaggero, M., and Mantelli, L. (2021). Parameter estimation of fire propagation models using level set methods. *Applied Mathematical Modelling*, 92:731–747. <https://doi.org/10.1016/j.apm.2020.11.030>.
- Atencia, M., Stoean, R., and Joya, G. (2020). Uncertainty quantification through dropout in time series prediction by echo state networks. *Mathematics*, 8:1374. <https://doi.org/10.3390/math8081374>.
- Banerjee, S., Carlin, B., and Gelfand, A. (2015). *Hierarchical Modeling and Analysis for Spatial Data*. Chapman & Hall/CRC, Boca Raton, FL, USA, 2 edition. <https://doi.org/10.1201/b17115>.
- Barredo Arrieta, A., Gil-Lopez, S., Laña, I., Bilbao, M. N., and Del Ser, J. (2022). On the post-hoc explainability of deep echo state networks for time series forecasting, image and video classification. *Neural Computing and Applications*, 34(13):10257–10277. <https://doi.org/10.1007/s00521-021-06359-y>.
- Bergstra, J. and Bengio, Y. (2012). Random search for hyper-parameter optimization. *Journal of Machine Learning Research*, 13:281–305.
- Bonas, M. and Castruccio, S. (2021). Calibration of spatial forecasts from citizen science urban air pollution data with sparse recurrent neural networks. *arXiv preprint arXiv:2105.02971*.
- Brotos, L., Aquilué, N., de Cáceres, M., Fortin, M.-J., and Fall, A. (2013). How fire history, fire suppression practices and climate change affect wildfire regimes in mediterranean landscapes. *PloS one*, 8(5):e62392. <https://doi.org/10.1371/journal.pone.0062392>.
- Burge, J., Bonanni, M. R., Hu, R., and Ihme, M. (2022). Recurrent convolutional deep neural networks for modeling time-resolved wildfire spread behavior. *arXiv preprint arXiv:2210.16411*.

- Cannon, S. and DeGraff, J. (2009). The increasing wildfire and post-fire debris-flow threat in western usa, and implications for consequences of climate change. In *Landslides – Disaster Risk Reduction*, pages 177–190. Springer. https://doi.org/10.1007/978-3-540-69970-5_9.
- Chen, S. and Billings, S. (1992). Neural networks for nonlinear dynamic system modelling and identification. *International Journal of Control*, 56(2):319–346. <https://doi.org/10.1080/00207179208934317>.
- Cressie, N. and Wikle, C. K. (2011). *Statistics for Spatio-Temporal Data*. Wiley, New Jersey.
- Dabrowski, J. J., Huston, C., Hilton, J., Mangeon, S., and Kuhnert, P. (2022a). Towards data assimilation in level-set wildfire models using bayesian filtering. *arXiv preprint arXiv:2206.08501*.
- Dabrowski, J. J., Pagendam, D. E., Hilton, J., Sanderson, C., MacKinlay, D., Huston, C., Bolt, A., and Kuhnert, P. (2022b). Bayesian physics informed neural networks for data assimilation and spatio-temporal modelling of wildfires. *arXiv preprint arXiv:2212.00970*.
- Daw, R. and Wikle, C. K. (2022). Reds: Random ensemble deep spatial prediction. *Environmetrics*, page e2780. <https://doi.org/10.1016/j.spasta.2020.100408>.
- Fendell, F. and Wolff, M. (2001). Wind-aided fire spread. In *Forest Fires: Behavior and Ecological Effects*, page 171–223. Academic Press. [10.1016/B978-012386660-8/50008-8](https://doi.org/10.1016/B978-012386660-8/50008-8).
- Fernández-López, J. (2022). rwind: Download, edit and include wind and sea currents data in ecological and evolutionary analysis. *R package version 1.1.7*.
- Gal, Y. and Ghahramani, Z. (2016). Dropout as a bayesian approximation: Representing model uncertainty in deep learning. *arXiv preprint arXiv:1506.02142*.
- George, E. and McCulloch, R. (1993). Variable selection via gibbs sampling. *Journal of the American Statistical Association*, 88:881–889. <https://doi.org/10.2307/2290777>.
- Geospatial Multi-Agency Coordination Group (2019). Historic perimeters combined 2000-2018 geomac. *Geospatial Multi-Agency Coordination Group*.
- Gibou, F., Fedkiw, R., and Osher, S. (2018). A review of level-set methods and some recent applications. *Journal of Computational Physics*, 353:82–109. <https://doi.org/10.1016/j.jcp.2017.10.006>.
- Gneiting, T. and Raftery, A. (2012). Strictly proper scoring rules, prediction, and estimation. *Journal of the American Statistical Association*, 102:359–378. <https://doi.org/10.1198/016214506000001437>.
- Hohner, A., Rhoades, C., Wilkerson, P., and Rosario-Ortiz, F. (2019). Wildfires alter forest watersheds and threaten drinking water quality. *Accounts of Chemical Research*, 52:1234–1244. DOI: [10.1021/acs.accounts.8b00670](https://doi.org/10.1021/acs.accounts.8b00670).
- Huang, H., Castruccio, S., and Genton, M. G. (2021). Forecasting high-frequency spatio-temporal wind power with dimensionally reduced echo state networks. *arXiv preprint arXiv:2102.01141*.

- Hyndman, R. J. (1996). Computing and graphing highest density regions. *The American Statistician*, 50:120–126. <https://doi.org/10.2307/2684423>.
- Lo, S.-E. (2012). A fire simulation model for heterogeneous environments using the level set method. *Claremont Graduate University, 2012 Ph.D. thesis*. [10.5642/cguetd/72](https://doi.org/10.5642/cguetd/72).
- Lukoševičius, M. (2012). A practical guide to applying echo state networks. In *Neural Networks: Tricks of the Trade*, pages 659–686. Springer. https://doi.org/10.1007/978-3-642-35289-8_36.
- Mallet, V., Keyes, D. E., and Fendell, F. E. (2009). Modeling wildland fire propagation with level set methods. *Computers and Mathematics with Applications*, 57(7):1089–1101. <https://doi.org/10.1016/j.camwa.2008.10.089>.
- Matzner, F. (2022). Hyperparameter tuning in echo state networks. *arXiv preprint arXiv:2207.07976*.
- McDermott, P. and Wikle, C. (2017). An ensemble quadratic echo state network for non-linear spatio-temporal forecasting. *Stat*, 6:315–330. <https://doi.org/10.1002/sta4.160>.
- McDermott, P. and Wikle, C. K. (2019). Deep echo state networks with uncertainty quantification for spatio-temporal forecasting. *Environmetrics*, 30:e2553. <https://doi.org/10.1002/env.2553>.
- Miller, C., Hilton, J., Sullivan, A., and Prakash, M. (2015). Spark—a bushfire spread prediction tool. In *International Symposium on Environmental Software Systems*, pages 262–271. Springer. [10.1007/978-3-319-15994-2_26](https://doi.org/10.1007/978-3-319-15994-2_26).
- Osher, S. and Fedkiw, R. (2002). *Level Set Methods and Dynamic Implicit Surfaces*. Springer-Verlag, New York. <https://doi.org/10.1007/b98879>.
- Osher, S. and Sethian, J. A. (1988). Fronts propagating with curvature dependent speed: Algorithms based on hamilton-jacobi formulations. *Journal of Computational Physics*, 79(1):12–49. [https://doi.org/10.1016/0021-9991\(88\)90002-2](https://doi.org/10.1016/0021-9991(88)90002-2).
- Probst, P., Boulesteix, A.-L., and Bischl, B. (2018). Tunability: Importance of hyperparameters of machine learning algorithms. *arXiv preprint arXiv:1802.09596*.
- Raissi, M., Perdikaris, P., and Karniadakis, G. E. (2019). Physics-informed neural networks: A deep learning framework for solving forward and inverse problems involving nonlinear partial differential equations. *Journal of Computational physics*, 378:686–707. <https://doi.org/10.1016/j.jcp.2018.10.045>.
- Ribeiro, G., Sauer, J., Fraccanabbia, N., Mariani, V., and Coelho, L. (2020). Bayesian optimized echo state network applied to short-term load forecasting. *Energies*, 13:2390. <https://doi.org/10.3390/en13092390>.
- Rothermel, R. C. (1972). A mathematical model for predicting fire spread in wildland fuels. *Res. Pap. INT-115*. Ogden, UT: U.S. Department of Agriculture, Intermountain Forest and Range Experiment Station.

- Sheng, C., Zhao, J., Wang, W., and Leung, H. (2013). Prediction intervals for a noisy nonlinear time series based on a bootstrapping reservoir computing network ensemble. *IEEE Transactions on Neural Networks and Learning Systems*, 24(7):1036–1048. [10.1109/TNNLS.2013.2250299](https://doi.org/10.1109/TNNLS.2013.2250299).
- Sivanandam, S. and Deepa, S. (2008). *Introduction to Genetic Algorithms*. Springer, Berlin. <https://doi.org/10.1007/978-3-540-73190-0>.
- Thiede, L. and Parlitz, U. (2019). Gradient based hyperparameter optimization in echo state networks. *Neural Networks*, 115:23–29. <https://doi.org/10.1016/j.neunet.2019.02.001>.
- Wikle, C. and Zammit-Mangion, A. (2022). Statistical deep learning for spatial and spatio-temporal data. *arXiv preprint arXiv:2206.02218*.
- Wikle, C. K., Datta, A., Hari, B. V., Boone, E. L., Sahoo, I., Kavila, I., Castruccio, S., Simmons, S. J., Burr, W. S., and Chang, W. (2022). An illustration of model agnostic explainability methods applied to environmental data. *Environmetrics*, page e2772.
- Wikle, C. K., Zammit-Mangion, A., and Cressie, N. (2019). *Spatio-Temporal Statistics with R*. Chapman & Hall/CRC, Florida.
- Wu, Q., Fokoue, E., and Kudithipudi, D. (2018). On the statistical challenges of echo state networks and some potential remedies. *arXiv preprint arXiv:1802.07369*.
- Yao, W., Zeng, Z., Lian, C., and Tang, H. (2013). Ensembles of echo state networks for time series prediction. In *2013 Sixth International Conference on Advanced Computational Intelligence (ICACI)*, pages 299–304. [10.1109/ICACI.2013.6748520](https://doi.org/10.1109/ICACI.2013.6748520).
- Yoo, M. and Wikle, C. K. (2022). A bayesian spatio-temporal level set dynamic model and application to fire front propagation. *arXiv preprint arXiv:2210.14978*.
- Yu, T. and Zhu, H. (2020). Hyper-parameter optimization: A review of algorithms and applications. *arXiv preprint arXiv:2003.05689*.
- Zhang, B., Miller, D. J., and Wang, Y. (2012). Nonlinear system modeling with random matrices: Echo state networks revisited. *IEEE Transactions on Neural Networks and Learning Systems*, 23(1):175–182. [10.1109/TNNLS.2011.2178562](https://doi.org/10.1109/TNNLS.2011.2178562).
- Zuo, Z., Shuai, B., Wang, G., Liu, X., Wang, X., Wang, B., and Chen, Y. (2015). Convolutional recurrent neural networks: Learning spatial dependencies for image representation. In *2015 IEEE Conference on Computer Vision and Pattern Recognition Workshops (CVPRW)*, pages 18–26. [10.1109/CVPRW.2015.7301268](https://doi.org/10.1109/CVPRW.2015.7301268).